Closed-loop Voltage Control of a GaN-based Modular Multilevel Clamped Capacitor Converter

Liyao Wu
School of Electrical and Computer Engineering
Georgia Institute of Technology
Atlanta, Georgia 30332–0250
Email: lwu49@gatech.edu

Maryam Saeedifard
School of Electrical and Computer Engineering
Georgia Institute of Technology
Atlanta, Georgia 30332–0250
Email: maryam@ece.gatech.edu

***Abstract*—The Modular Multilevel Clamped Capacitor Converter (MMC3) is an attractive switched-capacitor converter topology with desired features including high voltage conversion ratio, high power density and modularity. However, its application is hindered because of the lack of output voltage regulation. This paper proposes a closed-loop voltage control strategy for the MMC3 based on a detailed time-domain model of the converter. The proposed strategy relies on the impact of Pulse Dropping Technique (PDT) on the MMC3 conversion ratio to regulate the output voltage. A compact MMC3 prototype is designed and built with GaN FETs and tested up to 40 W. The developed model and proposed control strategy are validated by simulation and experimental studies.**

***Index Terms*—MMC3, GaN FETs, switched-capacitor converter, time-domain model, output voltage regulation**

I. Introduction

DC-DC converters with high voltage conversion ratio (CR) are attractive converters for a number of applications, such as data center power distribution system [1] and photo-voltaic energy conversion [2]. The conventional buck/boost converters have significant drawbacks for these applications due to extreme duty ratios and the usage of overrated components, leading to increased power losses and reduced power density. On the contrary, switched-capacitor power converters offer improved power density and system efficiency with high CR by eliminating the use of bulky inductors and using semiconductor devices with reduced rating values [3]. Among various switched-capacitor converter topologies, the Modular Multilevel Clamped Capacitor Converter (MMC3) stands out with several desirable features. In the MMC3 system, the power switches are only rated at 1 or 2 times of the low-side voltage [4]. With modular structure and reduced component voltage stress, GaN devices with relatively low voltage ratings that have demonstrated unique electrical and thermal capabilities/characteristics compared to their Si counterparts can be used for the MMC3 to further improve system efficiency and power density at high switching frequencies [5]–[9]. The MMC3 also features simple gate signals for power switches and enhanced system reliability with its modular and scalable structure [10].

Despite the aforementioned features of the MMC3, its application in power electronic systems is limited due to lack of accurate and flexible output voltage regulation [2]. Traditionally, the output voltage of the MMC3 can be only integer multiples/aliquots of the input voltage and the CR is not variable. The existing open-loop MMC3 cannot stabilize the output voltage when the converter is subjected to any transients/disturbances either in the source or output load [11]. A phase-shift control strategy is proposed in [12] and [13] to enable output voltage regulation and zero voltage switching for resonant MMC3. However, the complexity of both the topology and control for the MMC3 is increased. Furthermore, the proposed control method has not yet been explored in details and tested under both input- and output-side disturbances. An asymmetrical (n/m)X MMCCC is proposed in [14] which can realize all natural-number CRs. However, the CRs cannot be varied continuously and are limited to discrete numbers. Thus, the output voltage cannot be controlled to track any specific reference value and be regulated dynamically in the event of input- or load-side transients.

In this paper, first, a detailed time-domain model of the MMC3 is developed. Then, an effective feedback control strategy for the MMC3 based on the Pulse Dropping Technique (PDT) is proposed to fully exploit its advantages. The developed model and proposed strategy are validated by theoretical state-space analysis, simulation studies in the MATLAB/Simulink environment with the PLECS toolbox and experiments on a GaN-based MMC3 prototype.

II. Time-domain model of the MMC3

The circuit diagrams of an $(n+1)$-level MMC3 for boost and buck modes of operation are shown in Figs.1 (a) and (b), respectively. The MMC3 consists of n identical SubModules (SMs) with each SM comprised of one capacitor and 3 power switches. There is an additional switch at the high-voltage side of the converter and a large capacitor at the output. The theoretical output voltage of the MMC3 is equal to $(n+1)V_{low}$ for boost mode of operation and $V_{high}/(n+1)$ for buck mode. The MMC3, due to its modularity, can conceptually meet any voltage level requirement. Another feature of the MMC3 is its low complexity in control. There are only two complementary phases of operation for the MMC3. During Phase I, all switches labeled with odd numbers in Fig. 1 conduct while switches labeled with even numbers block, e.g., S1, S3 and S5 conduct while S2, S4 and S6 block. The

978-1-5386-1180-7/18/$31.00 ©2018 IEEE

opposite happens during Phase II. In addition, by considering redundant SMs in the system, the MMC3 can bypass any failed SM and continue its normal operation, which can enhance the system reliability [10].

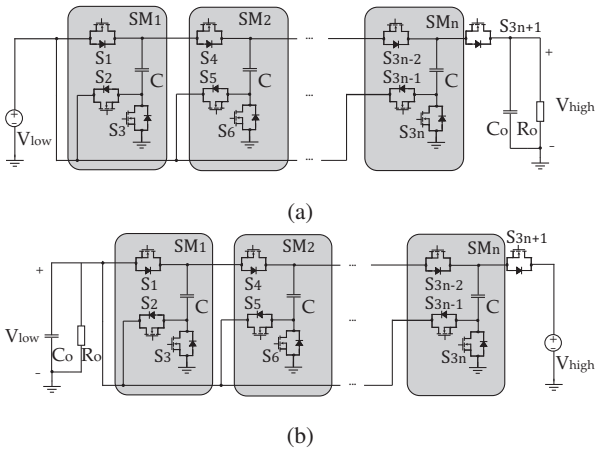

Fig. 1: Circuit diagrams of an $(n+1)$-level MMC3 for (a) boost and (b) buck modes of operation.

In order to understand the operation principle and performance of the MMC3 system, a detailed time-domain model is derived to express the output voltage, capacitor voltage ripples and current between the SMs as functions of load current, switching frequency and SM/output capacitances. Without loss of generality, a 5-level MMC3 system during boost mode of operation is used as an example. Fig. 2 shows the two switching states of the converter. During steady-state operation with open-loop control, the two states each lasts for a duration of $T/2$, where T is the switching period. During state (a), all switches labeled with odd numbers conduct and capacitors C_1 and C_3 get charged while C_2 and C_4 get discharged. During state (b), all switches labeled with even numbers conduct and C_2 and C_4 charge while C_1 and C_3 discharge.

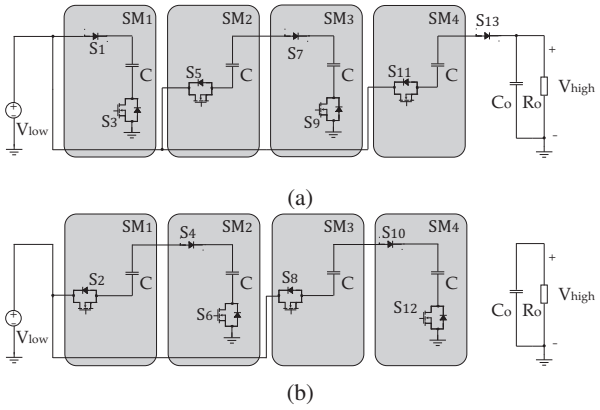

Fig. 2: Switching states of a 5-level MMC3 during boost operation with (a) odd-numbered on-state switches and (b) even-numbered on-state switches.

To derive the time-domain model of the MMC3 during steady-state operation under open-loop control, a set of assumptions are made as follows:

- the MMC3 system has a DC output voltage with very small ripple due to very high switching frequency,
- the SM capacitors have reached steady state prior to each switching state transition due to very small time constant,
- the net change of each capacitor voltage over one switching period is zero, i.e., $V_c(t+T) = V_c(t)$, and
- the output stage has a much larger time constant compared with that of a SM.

A. Output Voltage Ripple

Derivation of the time-domain model starts by determining the output voltage ripple accurately. Fig. 3 shows the output stage of MMC3 during the two switching states. During the state shown in Fig. 3(a), the output capacitor C_o gets charged with i_4 and discharged by the load current I_R. During the state shown in Fig. 3(b), C_o is discharged only by the load current. Thus, with the third assumption, i.e., capacitor charge balance, the following relationship holds for C_o:

$$\int_t^{t+\frac{T}{2}} i_4 dt - \int_t^{t+\frac{T}{2}} I_R dt = \int_{t+\frac{T}{2}}^{t+T} I_R dt. \qquad (1)$$

Based on (1) and the first assumption, we have

$$\int_t^{t+\frac{T}{2}} i_4 dt = \int_t^{t+T} I_R dt = I_R T = \frac{V_o}{R_o f}, \qquad (2)$$

where V_o is the output voltage and f is the switching frequency. Considering the fourth assumption, the output voltage ripple is determined by the charge from i_4:

$$\Delta V_o = \frac{\int_t^{t+\frac{T}{2}} i_4 dt}{C_o} = \frac{V_o}{R_o C_o f}. \qquad (3)$$

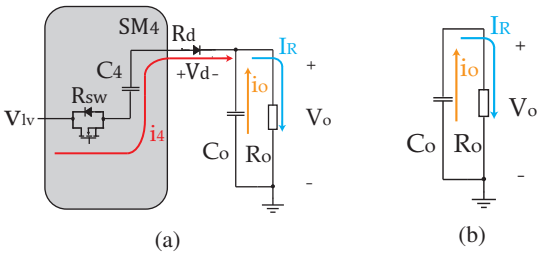

Fig. 3: Output stage of a 5-level MMC3 during boost operation with (a) odd-numbered on-state switches and (b) even-numbered on-state switches.

B. SM Capacitor Voltage Ripple

Based on (2), the voltage ripple of C_4 is:

$$\Delta V_4 = \frac{\int_t^{t+\frac{T}{2}} i_4 dt}{C_4} = \frac{V_o}{R_o C_4 f}. \qquad (4)$$

During the switching state shown in Fig. 2(b), capacitor C_3 charges C_4. As the capacitances are equal and they are in series, the voltage decrease of C_3 is equal to the voltage

increase of C_4, i.e., ΔV_3=ΔV_4. With the same procedure, it can be proved that all SM capacitors have the same voltage ripple magnitude. Thus, we have,

$$\Delta V_{SM} = \frac{V_o}{R_o C_{SM} f}, \tag{5}$$

where ΔV_{SM} is the voltage ripple magnitude of each SM capacitor and C_{SM} is the capacitance of SM capacitors.

C. Average Output Voltage

Based on the mathematical derivations for capacitor voltage ripples from Subsections II-A and II-B, the average output voltage of the MMC3 can be calculated.

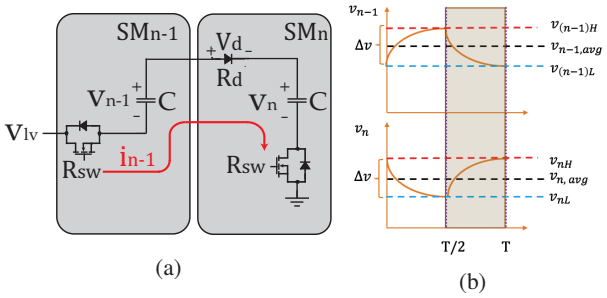

Fig. 4: (a) Typical connection diagram between two SMs and (b) their capacitor voltage waveforms.

A typical way of connection between two SMs in conjunction with the SM capacitor voltages of the MMC3 over one switching cycle are shown in Figs. 4 (a) and (b), respectively. In Fig. 4, V_{lv} is the supply voltage, V_d is the diode forward voltage drop, v_{nH}, $v_{n,avg}$ and v_{nL} represent the highest, average and lowest voltages of capacitor C_n, respectively, and $v_{(n-1))H}$, $v_{n-1,avg}$ and $v_{(n-1)L}$ represent the voltages of capacitor $C_{(n-1)}$. In the following analysis, it is assumed that the two SMs become connected after $t = T/2$. At the end of the switching cycle, the circuit has reached steady state and we have:

$$v_{nH} = V_{lv} + v_{(n-1)L} - V_d. \tag{6}$$

Based on Fig. 4(b),

$$v_{nH} = v_{n,avg} + \frac{\Delta V_{SM}}{2} \tag{7}$$

and

$$v_{(n-1)L} = v_{(n-1),avg} - \frac{\Delta V_{SM}}{2}. \tag{8}$$

Based on (6), (7) and (8), the average voltage of C_n is derived as

$$v_{n,avg} = V_{lv} + v_{(n-1),avg} - V_d - \Delta V_{SM}. \tag{9}$$

Following a similar procedure, the average capacitor voltage of the first SM and the average output voltage of the MMC3 can be expressed by

$$v_{1,avg} = V_{lv} - V_d - \frac{\Delta V_{SM}}{2}, \tag{10}$$

and

$$V_o = (n+1)V_{lv} - (n+1)V_d - n\Delta V_{SM} - \frac{\Delta V_o}{2}. \tag{11}$$

D. Stress of Components

During the design process of the MMC3, for proper component sizing, it is important to determine the voltage/current stresses of the components, i.e., switches and capacitors.

Based on the derivations in previous sections and Fig. 1, the maximum voltage of the capacitor C_n is nV_{lv}, and the maximum blocking voltage of the switches is V_{lv} for switches $S_{(3n+2)}, S_{(3n+3)}, n = 0, ..., 3$, and $S_{(3n+1)}, n = 0, 4$, and $2V_{lv}$ for switches $S_{(3n+1)}, n = 1, ..., 3$.

To determine the peak and RMS current stresses of the components, the maximum voltage mismatch between two capacitors of the connected SMs needs to be calculated. Based on Fig. 4(b), the the maximum mismatch between capacitor voltages occur at the point of switching transition and is equal to $2\Delta V_{SM}$. The peak current between the connected SMs is then derived as

$$I_{peak} = \frac{2\Delta V_{SM}}{2R_{sw} + R_d}, \tag{12}$$

where R_{sw} and R_d are on-state resistances of the switch and diode (or switch in reverse-conduction), respectively. Similarly, the peak currents into the first SM and last SM are derived as

$$I_{peak,first} = \frac{\Delta V_{SM}}{R_{sw} + R_d}, \text{and} \tag{13}$$

$$I_{peak,last} = \frac{(\Delta V_{SM} + \Delta V_o)}{R_{sw} + R_d}. \tag{14}$$

Based on the circuit analysis in Fig. 4(a) with Laplacian Transform, the instant current through the power devices at time t is calculated to be

$$i(t) = I_p e^{-\lambda t}, \tag{15}$$

and the RMS current is given by

$$I = I_p \sqrt{\frac{1 - e^{-\lambda T}}{2\lambda T}}, \tag{16}$$

where I_p is the peak current value from (12), (13) or (14) depending on the case and $\lambda = \frac{2}{(2R_{sw}+R_d)C_{SM}}$ for the connected SMs in the middle, $\lambda = \frac{2}{(R_{sw}+R_d)C_{SM}}$ for the first SM and $\lambda = \frac{C_{SM}+C_o}{(R_{sw}+R_d)C_{SM}C_o}$ for the last SM.

III. The Proposed Closed-loop Control of the MMC3

The output voltage of the MMC3 can be continuously modulated by using the PDT [15]. However, the PDT has never been considered for achieving closed-loop control and output voltage regulation of the MMC3. In addition, the mechanism and impacts of the PDT have not been thoroughly studied in previous work. In this section, the PDT is described in detail and its mechanism revealed by an updated time-domain model. A feedback control strategy is then proposed, which bases upon the PDT to regulate the output voltage. State-space small-signal models for both the open-loop MMC3 and MMC3 with the proposed control are derived and the effectiveness of the proposed control strategy is validated by the Bode plots and step responses.

A. The PDT

The PDT generates the gating signals of the switches by comparing a square wave with adjustable amplitude of m_a with a triangular wave with amplitude of 1 [15]. When the instantaneous value of the square wave is larger than the triangular wave, the output is high, and vice versa. m_a is in the range of 0 to 1. It has been shown in [15] that m_a has a significant impact on the CR of the MMC3 and the CR of the MMC3 can be varied within a range by varying m_a instead of being fixed by the SM number.

In order to understand and evaluate the performance of the PDT, the time-domain model is updated and the average output voltage of the MMC3 under the PDT is derived.

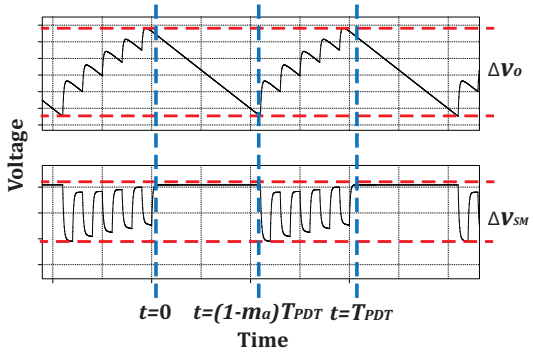

Fig. 5: Output voltage waveform (upper) and voltage of SM_n (lower) with $m_a = 0.5$ applied.

Figure. 5 shows the MMC3 output voltage waveform and the capacitor voltage of the last SM when $m_a = 0.5$.

The output voltage ripple can be expressed by

$$\Delta V_o = \frac{I_R(1-m_a)T_{PDT}}{C_o}. \tag{17}$$

In steady state, all SM capacitors have the same peak-to-peak voltage ripple. Based on capacitor charge balance, the ripple component of the SM capacitor voltage can be derived as

$$C_{SM}\frac{m_a T_{PDT}}{T}\Delta V_{SM} = I_R T_{PDT}, \tag{18}$$

$$\Delta V_{SM} = \frac{I_R T}{C_{SM} m_a} = \frac{V_o}{R_o C_{SM} m_a f}. \tag{19}$$

It can be seen that the ripple of SM capacitor voltages under the PDT is $\frac{1}{m_a}$ times larger than that in the original system as shown in equation (5). Thus, based on

$$V_o = (n+1)V_{lv} - (n+1)V_d - \frac{nI_R T}{C_{SM} m_a} - \frac{I_R(1-m_a)T_{PDT}}{2C_o}. \tag{20}$$

Considering the change in the period of time current flows between SMs under the PDT, the RMS current of the power devices is given by

$$I_{PDT} = \sqrt{\frac{I^2 m_a T_{PDT}}{T_{PDT}}} = I\sqrt{m_a}, \tag{21}$$

where I is calculated based on (16) with ΔV_o and ΔV_{SM} from (17) and (19), respectively .

From (20), it is evident that by varing m_a, the PDT can achieve an adjustable CR by adjusting the SM capacitor voltage ripple and output voltage ripple.

B. The Proposed PDT-based Feedback Control

Since the PDT method is capable of achieving non-integer CRs with a simple adjustment, it is proposed here to use this technique to achieve output voltage regulation for the MMC3. The proposed control strategy is demonstrated in Fig. 6. First, the output voltage of the MMC3 is measured and compared with the reference value. The difference goes through a PI controller and generates m_a for the PDT-based control. The gate signals for switches in the inserted SMs are obtained through a PWM between the high-frequency square wave with an amplitude of m_a and the low-frequency triangular waveform with an amplitude of 1. The output voltage is thus regulated by the feedback control loop. This method can regulate the output voltage of MMC3 during both boost and buck operation.

To evaluate the performance of the proposed control strategy, a small-signal state-space model of the converter is derived and the Bode diagrams of both the open-loop MMC3 system and the MMC3 with the proposed control strategy are studied. Without loss of generality, a 4-SM MMC3 in boost mode of operation is analyzed as an example. The results obtained can be easily extended to an MMC3 in buck mode of operation and/or with any number of SMs. In the state-space model, the voltage of each capacitor in the system is considered as a state variable. Input voltage, load current and m_a index are considered inputs to the system while the output voltage is considered as an output.

The Bode diagrams of the open-loop system are given in Fig. 7. Both the gains for input voltage and output current disturbances demonstrate large magnitude at low frequencies, which leads to steady state errors in the output voltage during

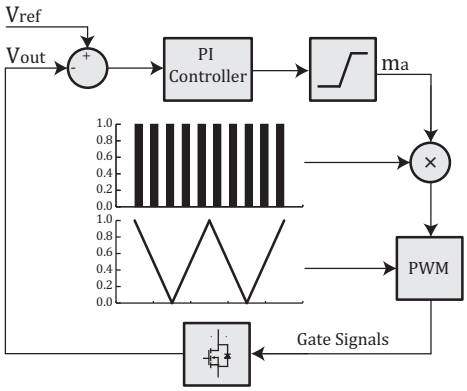

Fig. 6: The proposed feedback control designed for the MMC3 based on the PDT during boost operation.

step changes in the input voltage and load current. The Bode diagrams of the closed-loop system are given in Fig. 8. Unlike the open-loop system, significantly reduced gain magnitudes for both the input voltage and output current disturbances are observed at low frequencies, which allows the system to eliminate steady state errors in the output voltage against input voltage and load current disturbances.

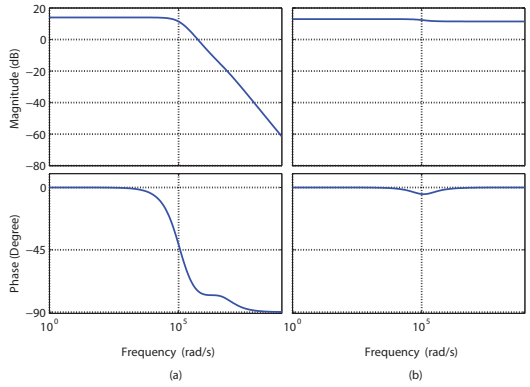

Fig. 7: Frequency response of the output voltage of the open-loop MMC3 with (a) input voltage and (b) load current.

The output voltage response to step changes in the load current for both the open-loop and closed-loop MMC3 based on the derived state-space model and parameters in Table I is demonstrated in Fig. 9. The load resistance is decreased from $100\ \Omega$ to $50\ \Omega$ in Fig. 9(a) and increased from $50\ \Omega$ to $100\ \Omega$ in Fig. 9(b). The results clearly demonstrate that the open-loop MMC3 cannot maintain the output voltage during load transients while the MMC3 with the proposed control strategy is able to properly maintain and regulate the output voltage.

IV. Simulation Results

Simulation study of an MMC3 system in boost operation has been carried out in the MATLAB/Simulink environment with the PLECS toolbox. Key parameters of the studies system are listed in Table II.

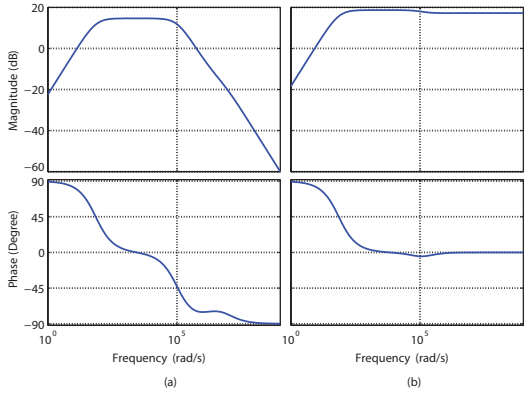

Fig. 8: Frequency response of the output voltage of the closed-loop MMC3 with (a) input voltage and (b) load current.

Parameter	Symbol	Value
Switching frequency	f	500 kHz
Input voltage	V_{lv}	4.42 V
SM capacitance	C	2.2 uF
Output capacitance	C_o	10 uF
Switch on-resistance	R_{sw}	20 mΩ
Diode on-resistance	R_d	20 mΩ
Diode forward voltage drop	V_d	0.7 V
Capacitor equivalent series resistance	R_C	10 mΩ
Propotional gain	K_p	0.1
Integral gain	K_i	100

TABLE I: System parameters for transfer function derivation

Based on the time-domain model of the MMC3, the voltages and currents are calculated theoretically according to the system parameters and compared with their corresponding simulation results in Table III. From Table III, the time-domain model is proved to provide very accurate results for the key values of the MMC3 performance.

To demonstrate the output regulation capability provided by the proposed strategy, simulation studies have been conducted for the MMC3 operating based on both open-loop and the proposed PDT feedback control strategy, with the input voltage subjected to a 0.5 V step-down change in one scenario and the output load subjected to a 100% step-up change in the other. Figure 10 shows the output voltage of the open-loop MMC3 when subjected to the step changes. In both cases, the system fails to maintain the output voltage, which is undesirable in most applications. Figures 11 (a) and (b) show the output voltage and m_a index profile of the MMC3 with the PDT feedback control under the two scenarios. As opposed to the open-loop system, in both cases, the MMC3 operating with the proposed control strategy is able to track a preset reference voltage of 45 V and maintain a constant output voltage by adjusting the m_a index after the transients.

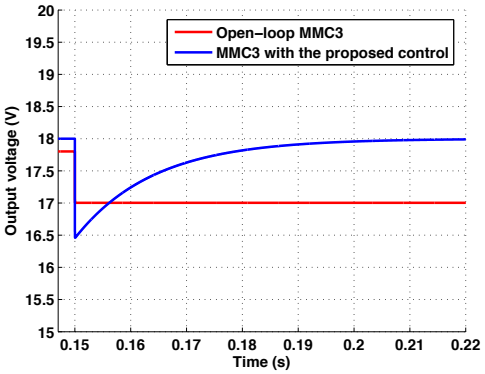

(a)

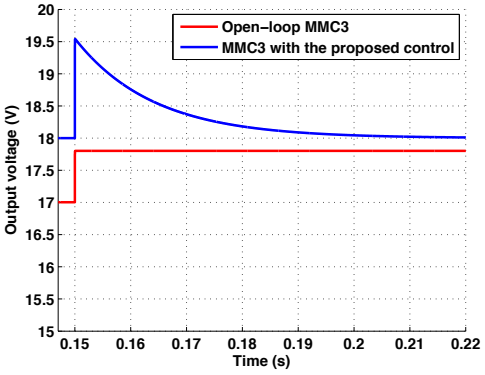

(b)

Fig. 9: Output voltage response of the open-loop and the closed-loop MMC3 to (a) a step-up and (b) a step-down change in the load current based on the derived transfer functions.

Parameter	Value
Input voltage	10 V
Output resistance	100 Ω
Total number of SMs	4
Switching frequency	500 kHz
m_f	10
SM capacitance	2.2 uF
Output capacitance	10 uF
Switch on-resistance	30 mΩ
Diode on-resistance	20 mΩ
Diode forward voltage drop	0 V

TABLE II: Parameters of the study system

V. Experimental results

To experimentally validate the developed time-domain model and evaluate the performance of the proposed control strategy, an MMC3 prototype based on GaN FETs is implemented. The developed MMC3 prototype is shown in Fig. 12(a) and the test setup is shown in Fig. 12(b). The control strategy is implemented in the TI F28069 microcontroller.

Figure 13 shows the steady-state output and switch gate voltage waveforms of the MMC3 obtained with an input DC voltage of 10 V and a load of 100 Ω. From the scope readings,

Parameter	Simulation	Model
Output voltage	48.23 V	48.16 V
Output voltage ripple	0.065 V	0.091 V
SM 4 capacitor voltage	38.45 V	38.425 V
SM 1 capacitor voltage	9.78 V	9.78 V
SM 2 capacitor voltage	19.34 V	19.325 V
SM capacitor voltage ripple	0.44 V	0.45 V
SM 1 capacitor peak current	9 A	9 A
SM capacitor peak current	11 A	11.25 A
Switch current RMS	1.63 A	1.686 A

TABLE III: Comparison of simulation results and time-domain model

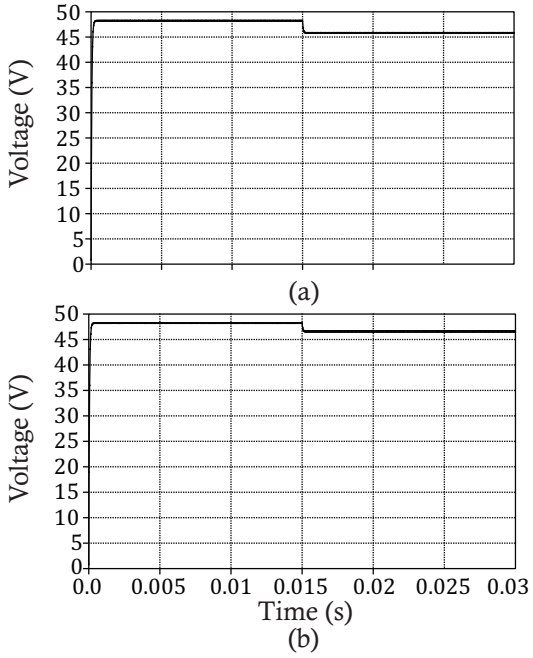

Fig. 10: The output voltage of an open-loop MMC3 when subjected to (a) source and (b) load step changes at $t = 0.015$s.

the frequency of the gate signals is 500 kHz and the output is 44.2 V, which is closely matched with the theoretical value of 44.16 V calculated with the time-domain model of the MMC3.

In order to validate the proposed control method, a TI microcontroller is programed to perform the PDT feedback control. The output voltage of the converter is read into the controller via an ADC port and the m_a index is adjusted by a PI function. Experiments are carried out with 5 V input voltage, 18 V output voltage reference and a 100 Ω load. While in the open-loop system, the output voltage will change as the input voltage changes, in the closed-loop system, as shown in Fig. 14, when input voltage is increased from 4.42 V to 5.02 V, the output voltage still accurately tracks the reference voltage of 18 V by adjusting m_a. This verifies the effectiveness of the proposed strategy to reject source voltage disturbance. Figures 15 (a) and (b) show the output voltage of the MMC3 under the PDT feedback and open-loop control strategies, respectively, during load-change scenarios. As shown, the output voltage in the open-loop case changes

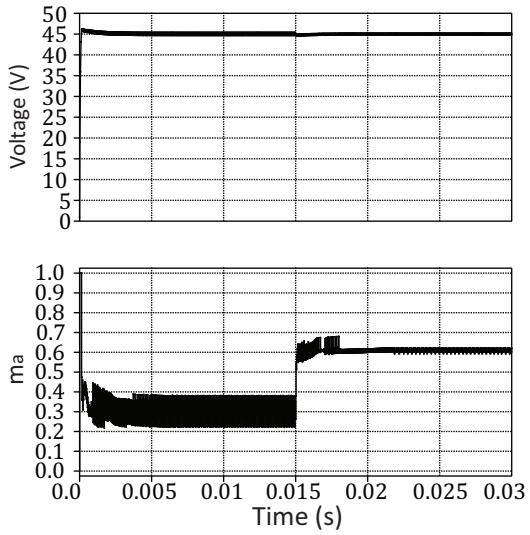

(a)

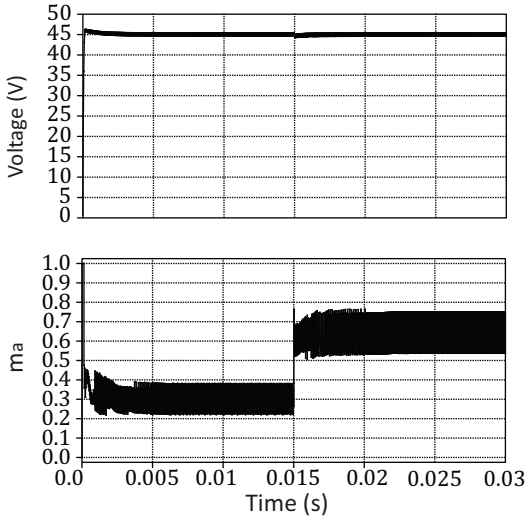

(b)

Fig. 11: Output voltage (upper) and m_a profile (lower) of the MMC3 operating based on the proposed PDT feedback control when subjected to (a) source voltage drop at $t = 0.015$ s and (b) load step change at $t = 0.015$ s.

during a load-change and the system is not able to return to its previous setpoint. On the contrary, in both cases, the system with the proposed control strategy is able to maintain the output voltage regulated at referenced value within 0.1 s time.

VI. Conclusion

In this paper, a detailed time-domain model for the MMC3 in conjunction with a closed-loop voltage control strategy based on the PDT are developed. The developed model provides very accurate results, which are verified by simulation and experimental results based on a GaN-based MMC3 prototype. To demonstrate effectiveness of the proposed control

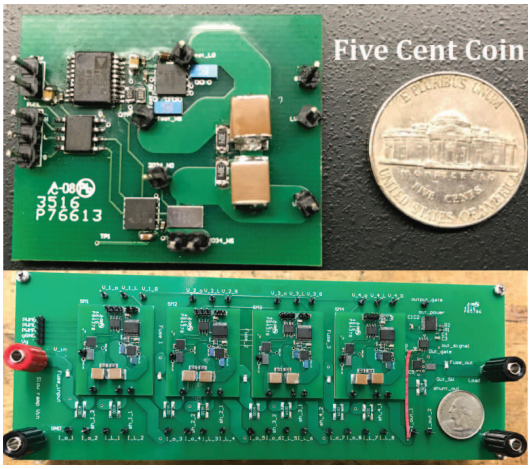

(a)

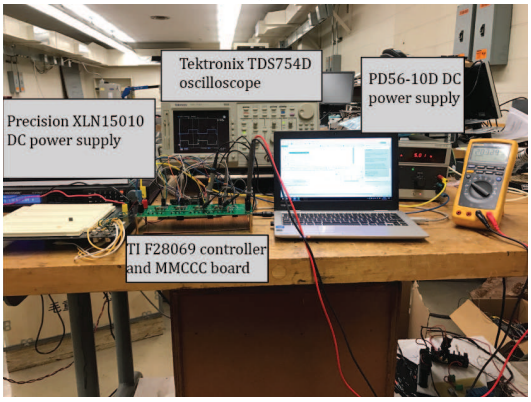

(b)

Fig. 12: (a) The SM board and the MMC3 prototype and (b) test setup with the MMC3 prototype.

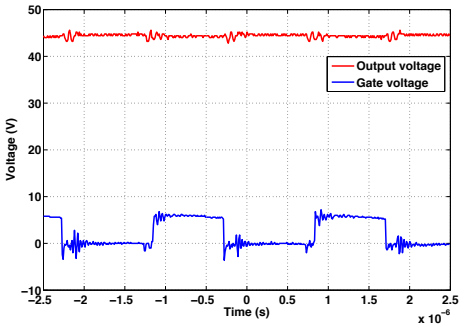

Fig. 13: Waveform of MMC3 output voltage and switch gate signal at 500 kHz with an input voltage of 10 V and a load of 100 Ω.

strategy, state-space small-signal models and Bode plots are studied for both the open-loop MMC3 and the MMC3 with the proposed method. The theoretical analysis and simulation/experimental results confirm that the MMC3 system with the proposed PDT feedback control strategy exhibits output voltage regulation capability against both source-side and load-side disturbances.

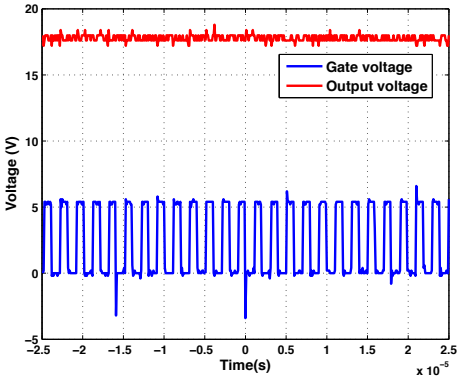

(a)

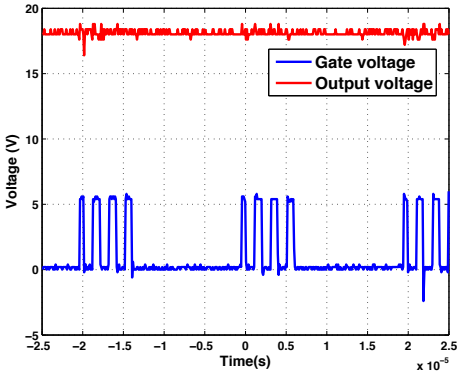

(b)

Fig. 14: Output voltage and the PDT gate signal of the MMC3 with an output voltage reference of 18 V and input voltage of (a) 4.42 V and (b) 5.02 V.

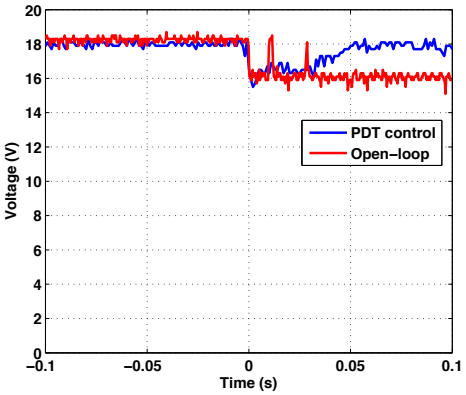

(a)

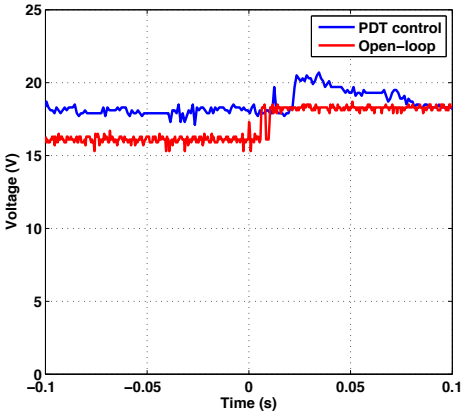

(b)

Fig. 15: The output voltage of the MMC3 under the PDT feedback and open-loop control strategies when subjected to a load resistance change from (a) 100 Ω to 50 Ω and (b) 50 Ω to 100 Ω.

REFERENCES

[1] Y. Cui, W. Zhang, L. M. Tolbert, F. Wang, and B. J. Blalock, "Direct 400 V to 1 V converter for data center power supplies using GaN FETs," in *IEEE Applied Power Electronics Conference and Exposition (APEC)*, 2014, pp. 3460–3464.

[2] M. Kasper, M. Ritz, D. Bortis, and J. W. Kolar, "PV panel-integrated high step-up high efficiency isolated GaN DC-DC boost converter," in *35th International Telecommunications Energy Conference 'Smart Power and Efficiency' (INTELEC)*, 2013, pp. 1–7.

[3] Y. Lei, R. May, and R. Pilawa-Podgurski, "Split-phase control: Achieving complete soft-charging operation of a Dickson switched-capacitor converter," *IEEE Trans. Power Electron.*, vol. 31, no. 1, pp. 770–782, 2016.

[4] D. Cao, X. Lyu, and Y. Li, "Multilevel modular converter with reduced device count for hybrid and electric vehicle," in *IEEE Transportation Electrification Conference and Expo (ITEC)*, 2015, pp. 1–6.

[5] A. Lidow, J. Strydom, M. D. Rooij, and D. Reusch, *GaN transistors for efficient power conversion*, 2nd ed. John Wiley & Sons, 2014.

[6] J. Millan, P. Godignon, X. Perpina, A. Prez-Toms, and J. Rebollo, "A survey of wide bandgap power semiconductor devices," *IEEE Trans. Power Electron. on*, vol. 29, no. 5, pp. 2155–2163, 2014.

[7] H. A. Mantooth, M. D. Glover, and P. Shepherd, "Wide bandgap technologies and their implications on miniaturizing power electronic systems," *IEEE Trans. Emerg. Sel. Topics Power Electron.*, vol. 2, no. 3, pp. 374–385, 2014.

[8] J. A. Ferreira, J. Popovic, J. D. van Wyk, and F. Pansier, "System integration of GaN technology," in *IEEE International Power Electronics Conference (IPEC)*, 2014, pp. 1935–1942.

[9] L. Tolbert, B. Ozpineci, S. Islam, and M. Chinthavalli, "Wide bandgap semiconductors for utility applications," in *Proceeding of Power and Energy Systems*, 2003.

[10] F. H. Khan and L. M. Tolbert, "Multiple-Load–Source Integration in a Multilevel Modular Capacitor-Clamped DC–DC Converter Featuring Fault Tolerant Capability," *IEEE Trans. Power Electron.*, vol. 24, no. 1, pp. 14–24, 2009.

[11] F. H. Khan, L. M. Tolbert, and W. E. Webb, "Start-Up and dynamic modeling of the multilevel modular capacitor-clamped converter," *IEEE Trans. Power Electron.*, vol. 25, no. 2, pp. 519–531, 2010.

[12] D. Cao, X. Lu, X. Yu, and F. Z. Peng, "Zero voltage switching double-wing multilevel modular switched-capacitor dc-dc converter with voltage regulation," in *Twenty-Eighth Annual IEEE Applied Power Electronics Conference and Exposition (APEC)*, 2013, pp. 2029–2036.

[13] Y. Li, B. Curuvija, X. Lyu, and D. Cao, "Multilevel modular switched-capacitor resonant converter with voltage regulation," in *IEEE Applied Power Electronics Conference and Exposition (APEC)*, 2017, pp. 88–93.

[14] G. Han, D. Gunasekaran, L. Qin, and F. Z. Peng, "Asymmetrical (n/m)X DC-DC converter for finer voltage regulation," in *IEEE Applied Power Electronics Conference and Exposition (APEC)*, 2017, pp. 99–106.

[15] M. K. Alam and F. H. Khan, "Efficiency Characterization and Impedance Modeling of a Multilevel Switched-Capacitor Converter Using Pulse Dropping Switching Scheme," *IEEE Trans. Power Electron.*, vol. 29, no. 6, pp. 3145–3158, 2014.